

# Evolution of electronic structure of doped Mott insulators - reconstruction of poles and zeros of Green's function

Shiro Sakai, Yukitoshi Motome, and Masatoshi Imada

Department of Applied Physics, University of Tokyo, Hongo, Tokyo 113-8656, Japan

(Dated: October 22, 2018)

We study evolution of metals from Mott insulators in the carrier-doped 2D Hubbard model using a cluster extension of the dynamical mean-field theory. While the conventional metal is simply characterized by the Fermi surface (pole of the Green function  $G$ ), interference of the *zero surfaces* of  $G$  with the pole surfaces becomes crucial in the doped Mott insulators. Mutually interfering pole and zero surfaces are dramatically transferred over the Mott gap, when lightly doped holes synergetically loosen the doublon-holon binding. The heart of the Mott physics such as the pseudogap, hole pockets, Fermi arcs, in-gap states, and Lifshitz transitions appears as natural consequences of this global interference in the frequency space.

PACS numbers: 71.10.Hf; 71.30.+h; 74.72.-h

Electronic structures of doped Mott insulators have intensively been debated since the discovery of high- $T_c$  cuprates. While overdoped metals behave like a conventional Fermi liquid, an outstanding issue is how such metals evolve into the Mott insulator. Experimental studies on the doped cuprates revealed anomalous metallic behaviors in the proximity to the Mott insulator. Among them angle-resolved photoemission spectroscopy (ARPES) found arclike spectra around the nodal points of the momenta  $\mathbf{k} = (\pm\frac{\pi}{2}, \pm\frac{\pi}{2})$ , with a pseudogap in the antinodal region of the Brillouin zone [1]. Moreover the high-resolution ARPES [2] and quantum oscillations of resistivity observed under magnetic fields [3] suggested the existence of a small closed Fermi surface, called the pocket, in contrast to the large surface expected in the normal Fermi liquid. These imply emergence of non Fermi liquids under a radical evolution of electronic structure upon doping.

Diverse theoretical proposals were made for the Mott physics of the 2D Hubbard model: The pseudogap was reproduced in various theoretical frameworks [4–6]. The exact diagonalization (ED) studies [7] further suggested a spectral weight transfer with doping from the upper Hubbard band (UHB) to the upper edge of the lower Hubbard band (LHB), which created in-gap states. The arc structure of the spectral weight was reproduced in the cluster perturbation theory [8], the dynamical cluster approximation [9, 10], and the cellular dynamical mean-field theory (CDMFT) [6, 11–13]. Hole-pocket Fermi surfaces around the nodal points were suggested in a phenomenology [14], the CDMFT [12], and a variational-cluster approach [15]. A topological change of the Fermi surface, i.e., Lifshitz transition [16], from electronlike to holelike surfaces due to a correlation effect was analyzed [17, 18]. A Lifshitz transition to electron pockets was also found upon electron doping [19]. In spite of these achievements, a coherent picture of the Mott physics has not emerged yet.

In general, poles of the single-particle Green function  $G(\mathbf{k}, \omega)$  are known to define the Fermi surface at the frequency  $\omega = 0$ . While  $\text{Re } G$  changes its sign across a pole through  $\pm\infty$ ,  $\text{Re } G$  may also change the sign across a *zero* defined by  $G = 0$ . Recent studies suggest, in addition to the poles, zeros of  $G$  play important roles [12, 14, 20]. In the Mott

insulator, the self-energy  $\Sigma(\mathbf{k}, \omega)$  inside the gap diverges on a specific surface in the  $\mathbf{k}$ - $\omega$  space, which defines a zero surface of  $G$ . Since the Fermi surface disappears in the Mott insulator while the zero surface appears instead, the evolution of the zeros makes crucial effects at low doping and is imperative in understanding the Mott physics.

In this letter we study the 2D Hubbard model using the CDMFT+ED method [12], and clarify the doping evolution of poles and zeros of  $G$  in the  $\mathbf{k}$ - $\omega$  space. By figuring out reconstruction of interfering poles and zeros in a wide  $\omega$  range, fragmentary features are integrated into a coherent understanding of the Mott physics at and around  $\omega = 0$ , namely, the hole-pocket Fermi surface, Fermi arc, pseudogap, in-gap states, and Lifshitz transitions. Starting from a high-energy structure in the scale of the Mott gap, we zoom in lower-energy hierarchy, in a clear and visible fashion, revealing two structures induced by hole doping. One is in-gap states formed above the occupied states separated by a pseudogap. The other is hole pockets in the nodal directions, which appear at the top of the occupied states below the pseudogap. The pseudogap is described by a zero surface crossing the Fermi level. The density-of-states analysis suggests that these structures result from a dramatic transfer of the weight over the Mott gap: This is caused by tiny doping, which loosens the doublon-holon binding. Then the zero surface interferes with the poles and pushes down the pole surface near the zeros below the Fermi level, leaving hole pockets around  $(\pm\frac{\pi}{2}, \pm\frac{\pi}{2})$ , which are more stabilized by the next-nearest transfer. With further doping, the Fermi surfaces undergo at least two continuous Lifshitz transitions before reaching a normal Fermi liquid with an electronlike Fermi surface.

The Hubbard Hamiltonian on a square lattice reads

$$H = \sum_{\mathbf{k}\sigma} \epsilon(\mathbf{k}) c_{\mathbf{k}\sigma}^\dagger c_{\mathbf{k}\sigma} - \mu \sum_{i\sigma} n_{i\sigma} + U \sum_{i\sigma} n_{i\uparrow} n_{i\downarrow}, \quad (1)$$

where  $c_{\mathbf{k}\sigma}$  ( $c_{\mathbf{k}\sigma}^\dagger$ ) destroys (creates) an electron of spin  $\sigma$  with momentum  $\mathbf{k}$ , and  $n_{i\sigma}$  is a spin density operator at site  $i$ .  $U$  represents the onsite Coulomb repulsion,  $\mu$  the chemical potential, and  $\epsilon(\mathbf{k}) = -2t(\cos k_x + \cos k_y) - 4t' \cos k_x \cos k_y$ , where  $t$  ( $t'$ ) is the (next-)nearest-neighbor transfer integral.

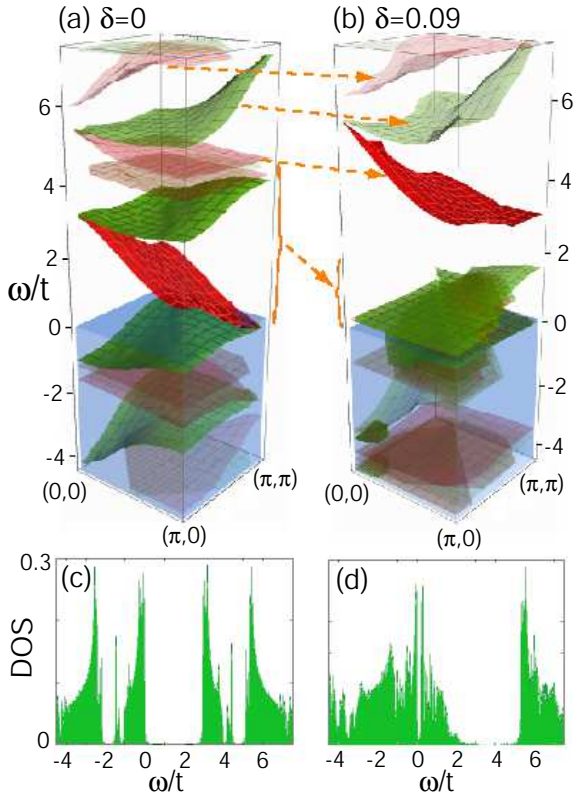


FIG. 1: The  $\mathbf{k}$ - $\omega$  structure of poles and zeros of  $G$  for  $t' = 0$ ,  $U = 8t$  at (a)  $\delta=0$  and (b) 0.09. Poles (zeros) are plotted in green (red). Occupied regions for an electron are filled with aqua. The transparency of pole (zero) surfaces reflects the imaginary part of the (inverse) self-energy (more transparent for larger imaginary part). (c) and (d) show the density of states per spin at  $\delta = 0$  and 0.09, respectively.

In the CDMFT, the infinite lattice of the model (1) is self-consistently mapped onto an  $N_c$ -site cluster embedded in infinite bath sites, which define an  $N_c \times N_c$  dynamical mean-field matrix  $g_0(i\omega_n)$  for the cluster in terms of Matsubara frequency  $\omega_n$ . We employ the ED method with the Lanczos algorithm to solve the cluster problem at zero temperature, where  $g_0$  is fitted with a finite number of bath parameters and a fictitious temperature  $1/\beta$  is introduced. We adopt 2 by 2 cluster ( $N_c = 4$ ) coupled with 8 bath sites and  $\beta = 100/t$  unless otherwise mentioned. When a self-consistency loop converges, we obtain an  $N_c \times N_c$  self-energy matrix  $\Sigma_c(i\omega_n)$ , whose elements are defined on sites within the cluster. Then we interpolate cluster quantities in the momentum space, to obtain the original infinite-lattice ones. To study poles and zeros of  $G$  simultaneously, after careful examination, we employ a suitable scheme of the cumulant periodization [12], where the cluster cumulant  $M_c \equiv (i\omega_n + \mu - \Sigma_c)^{-1}$  is interpolated with a Fourier transformation cut by a cluster size  $N_c$ ,

$$M(\mathbf{k}, i\omega_n) = \frac{1}{N_c} \sum_{i,j=1}^{N_c} [M_c(i\omega_n)]_{ij} e^{i\mathbf{k} \cdot (\mathbf{x}_i - \mathbf{x}_j)}. \quad (2)$$

After  $M$  is obtained,  $G$  and  $\Sigma$  on the original lattice are cal-

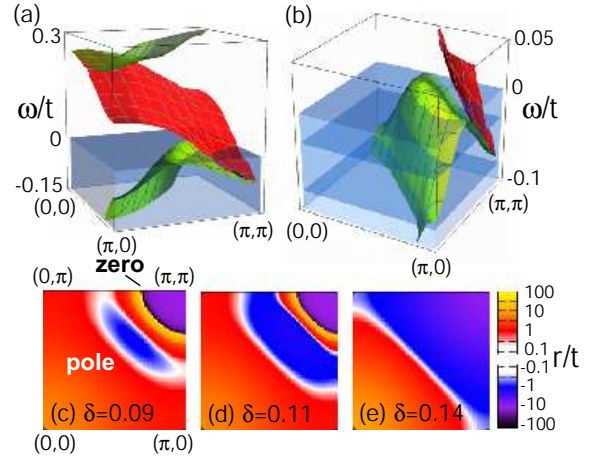


FIG. 2: (a)(b) Close-ups of Fig. 1(b) at two different lower-energy scales. Blue grade levels in (b) depict rigid-band shifts of the chemical potential. (c)(d)(e)  $r(\mathbf{k}) \equiv \text{Re}[G^{-1}(\mathbf{k}, 0)]$  in the first quadrant of the Brillouin zone for  $t' = 0$  and  $U = 8t$  at  $\delta = 0.09, 0.11$  and 0.14, respectively.  $r = 0$  ( $\pm\infty$ ) defines the Fermi surface (the zero surface of  $G$ ). We set  $\eta = 10^{-4}t$  for these data.

culated with  $G = [M^{-1} - \epsilon(\mathbf{k})]^{-1}$  and  $\Sigma = i\omega_n + \mu - M^{-1}$ , respectively. The Lanczos-ED method allows us to calculate  $G$  at real frequencies directly through a continued-fraction expansion [21], where a Matsubara frequency  $i\omega_n$  is replaced by  $\omega + i\eta$  with a small positive factor  $\eta$ . Although we should be careful on the limitation of the present size of the cluster, this combination of the methods is appropriate as the state of the art in exploiting zero and pole structures on equal footing in a wide spectrum range.

We start from electronic structure of the Mott insulator at half filling ( $\delta = 0$ ;  $\delta$  is the hole doping rate from half filling) for  $t' = 0$  and  $U/t = 8$ . While an insulating phase caused by some symmetry breaking may show a similar feature, to capture the essence of the Mott physics, we assume a paramagnetic solution in the CDMFT. Figure 1(a) shows the structure of poles (green surfaces) and zeros (red surfaces) of  $G$  in the  $\mathbf{k}$ - $\omega$  space. Here  $\omega$  is measured from the upper edge of the occupied states [22] to compare with the doped case below. The zero surface around  $0 < \omega < 3t$  (the most distinct red surface) represents the Mott gap, which separates UHB and LHB displayed by entangled pole and zero surfaces. The zero surface at the Mott gap touches the pole surfaces of the UHB (LHB) around  $(0,0)$  [ $(\pi, \pi)$ ] at  $\omega \simeq 3t$  ( $\omega \simeq 0$ ). The distinct pole surface in the UHB persists up to  $\omega \sim 4t$ , and another distinct one appears around  $5t < \omega < 7t$ . In accordance with these pole surfaces, there are large weights in the density of states (DOS) per spin [Fig. 1(c)]. In other area, poles are disrupted due to a large imaginary part of the self-energy, making incoherent contributions.

We next dope holes. Comparing the result at  $\delta = 0.09$  in Fig. 1(b) with Fig. 1(a), we see that high-energy ( $|\omega| \gtrsim 5t$ ) structure does not change appreciably while the lower-energy ( $|\omega| \lesssim 5t$ ) structure does: The pole surface at the bottom of

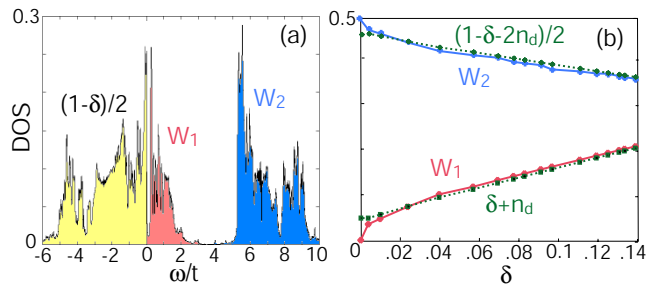


FIG. 3: (Color online) (a) DOS at  $\delta = 0.09$  [the same as Fig. 1(d)] and the definitions of weights  $W_1$  and  $W_2$ . (b)  $\delta$  dependence of  $W_1$  and  $W_2$  compared with the weights estimated from a simple analysis given by dashed lines (see the text). We set  $\eta = 10^{-2}t$  for these data.

UHB just above the Mott gap  $\sim 3t$  in Fig. 1(a) is transferred to the lowest-energy pole surface in the piles above  $\omega \simeq 0.2t$ , squashing the zero surface just below it, as in Fig. 1(b) and as will be seen in Figs. 2(a) and (b). In addition, one of vague zero surfaces in the UHB piles in Fig. 1(a) turns to a distinct one at around  $\omega = 4t$  in Fig. 1(b). Corresponding to these reconstructions, the DOS at  $\omega \simeq 3t$  in Fig. 1(c) is transferred to energies lower than  $\omega \simeq 2t$  as shown in Fig. 1(d).

Let us focus on a low-energy structure of poles and zeros. Figures 2(a) and (b) provide enlarged views of Fig. 1(b) near the Fermi level, in two different energy scales. A prominent feature is a small gap, described by a zero surface cutting the Fermi level. The gap has a small width of  $\sim 0.2t$ , and is distinguished from the larger gap between the doped hole states and the UHB as shown in DOS in Fig. 1(d). A comparable pseudogap was found in earlier CDMFT studies [6, 12].

As the zero surface around  $(\pi, \pi)$  extends to the region  $\omega < 0$ , near the zero surface, the pole surface is pushed down below the Fermi level [Fig. 2(b)], because a zero and a pole surfaces cannot cross each other. Meanwhile in the regions far away from zeros, the energy of poles increases with  $|\mathbf{k}|$ , reflecting the original dispersion  $\epsilon(\mathbf{k})$ . Hence, along the direction from  $(0,0)$  to  $(\pi, \pi)$  for example, the pole energy initially increases, crossing the Fermi level, and then turns down around  $(\frac{\pi}{2}, \frac{\pi}{2})$ , crossing the Fermi level again. As a consequence, a hole pocket is formed around  $(\frac{\pi}{2}, \frac{\pi}{2})$ , accompanying a zero surface around  $(\pi, \pi)$ , as found previously in Ref. 12 and also shown in Fig. 2(c).

The metal-insulator transition occurs when the hole pockets shrink and vanish, indicating a topological nature of this transition [23]. Since the quick evolution for  $\delta \lesssim 0.01$  elucidated below suggests a proximity to the first-order transition, the marginal quantum criticality [23] may have relevance.

To get further insight into the underlying physics of the dramatic restructuring, we study the doping evolution of DOS systematically. We calculate the weight integrated over energy ranges of  $0 < \omega < 2.8t$  (in-gap weight),  $W_1$ , and that over  $2.8t < \omega < \infty$  (UHB weight),  $W_2$  [see Fig. 3(a)]. Figure 3(b) depicts  $\delta$  dependences of  $W_1$  and  $W_2$ , where  $W_1$  ( $W_2$ ) monotonically increases (decreases) with  $\delta$ .

As shown in Fig. 3(b), the in-gap weight  $W_1$  shows good agreement with  $\delta + n_d$ , where  $n_d \equiv \langle n_{i\uparrow}n_{i\downarrow} \rangle$  is the doublon density. It is natural to have the weight proportional to  $\delta$  in the rigid band picture because it comes from the holes doped into the LHB, but there is an additional contribution scaled by  $n_d$ . This is interpreted as a strong-correlation effect as follows. Neglecting dynamical fluctuations, we can roughly estimate the single-occupancy weight as  $W_0 \equiv \frac{1}{2} \sum_{\sigma} (n_{\sigma} - n_d) = \frac{1}{2}(1 - \delta - 2n_d)$ , where  $n_{\sigma} \equiv \langle n_{i\sigma} \rangle$  ( $\sigma = \uparrow, \downarrow$ ) is the spin density. Now, one electron added to these singly occupied states makes a ‘‘doublon’’ and contributes to the DOS of the UHB. This contribution should agree with  $W_2$ . Since the DOS below the Fermi level has a weight  $\frac{1}{2}(1 - \delta)$ , the remaining weight, which should be equal to  $W_1$ , becomes  $1 - \frac{1}{2}(1 - \delta - 2n_d) - \frac{1}{2}(1 - \delta) = \delta + n_d$ . This simple analysis explains well the overall behavior of  $W_1$  and  $W_2$ , as seen in Fig. 3(b).

A nontrivial finding, however, is that the weight  $n_d$  in  $W_1$  is very quickly transferred from the UHB to the top of LHB by tiny doping  $\delta \lesssim 0.01$  to the Mott insulator. Actually, the above simple analysis breaks down at very small  $\delta$ , where  $W_1$  eventually and obviously vanishes toward  $\delta = 0$  as shown in Fig. 3(b). At  $\delta = 0$ , this weight  $n_d$  is included in the UHB weight  $W_2$  and is interpreted as an electron excitation added to a holon tightly bound with a doublon. The number of doublons and holons should be the same in the Mott insulator and they are tightly bound with the binding energy equal to the Mott gap  $\sim 3t$ . Therefore one electron added to a hole site requires dissolution of the bound state and overcoming the Mott gap. The quick transfer of  $n_d$  from  $W_2$  to  $W_1$  means that the doublon-holon binding energy is quickly reduced from  $\sim 3t$  to  $\sim 0.2t$  presumably because of an efficient screening of the doublon-holon interaction by the doped holes. Even with this screening, the binding energy though small still survives as the pseudogap. This quick reduction is promoted by a positive feedback, because the dissolved bound pairs further join in screening other bound pairs. This constitutes a mechanism for the drastic restructuring in the Mott physics.

The next issue is how the hole-pocket Fermi surface accompanied by zeros of  $G$  in Fig. 2(c) evolves into a single electronlike Fermi surface expected in the normal Fermi liquid as  $\delta$  increases further. Figures 2(c), (d), and (e) depict  $r(\mathbf{k}) \equiv \text{Re}[G^{-1}(\mathbf{k}, 0)]$  at  $\delta = 0.09, 0.11$ , and  $0.14$ , respectively, showing how Fermi (zero) surfaces at  $r = 0$  ( $\pm\infty$ ) evolve. As  $\delta$  increases from  $0.09$ , the hole pocket continues to expand until it touches the Brillouin zone boundary ( $|k_x| = \pi$  or  $|k_y| = \pi$ ). When it touches the boundary, it changes into two concentric Fermi surfaces around  $(\pi, \pi)$  through a Lifshitz transition, while the zero surface remains around  $(\pi, \pi)$  [Fig. 2(d)]. Further doping enlarges the unoccupied region (blue region) sandwiched by the two concentric Fermi surfaces. Then, the smaller Fermi surface around  $(\pi, \pi)$  merges with the zero surface and they are annihilated in pair, leaving a large hole-like Fermi surface, which almost simultaneously transforms into a normal electronlike one through another Lifshitz transition [Fig. 2(e)]. For  $\delta \geq 0.14$  only a large electronlike Fermi surface is found. This evolution of Fermi and zero surfaces is

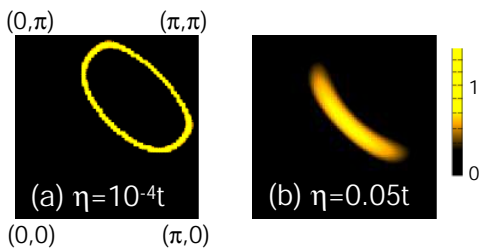


FIG. 4: (Color online)  $A(\mathbf{k}, 0) \equiv -\text{Im}[G(\mathbf{k}, \omega + i\eta)]/\pi$  for  $t' = -0.2t$ ,  $U = 12t$ , and  $\delta = 0.09$  with (a)  $\eta = 10^{-4}t$  and (b)  $\eta = 0.05t$ . Here we set the fictitious temperature  $1/\beta = t/200$ .

understood in a rigid band picture for the electronic structure in Fig. 2(b), as drawn with blue grade levels, if we assume that the hole doping only lowers the Fermi level without changing the structure of poles and zeros. Detailed inspection of the two Lifshitz transitions shows continuities of the electron density as a function of  $\mu$  and hence continuous transitions.

Apparently, the Luttinger sum rule [24] is violated for  $\delta \lesssim 0.11$  while roughly satisfied for  $\delta \gtrsim 0.14$ . Since the Luttinger theorem assumes an adiabatic continuity, there is no reason that the rule should be satisfied beyond the Lifshitz transition around  $\delta = 0.14$ . Other numerical calculations also pointed out the violation at small  $\delta$  [12, 17, 18].

Next we consider effects of  $t'$ . Results for  $\delta = 0.09$  (not shown) exhibits that  $t' < 0$  elevates (lowers) the energy of poles around the nodal direction [around  $(\pi, 0)$  and  $(0, \pi)$ ], as expected from the original dispersion  $\epsilon(\mathbf{k})$ . The enhancement around the nodal direction more stabilizes the hole-pocket structure while the reduction around  $(\pi, 0)$  and  $(0, \pi)$  more stabilizes a single holelike Fermi surface. Quantitative modifications caused by nonzero  $t'$  will be reported elsewhere.

Finally we discuss how a Fermi arc emerges in the lightly doped region. Stanescu and Kotliar found that the zero surface reduces the spectral weight from the neighboring Fermi surface, resulting in a Fermi arc [12]. In the present Lanczos-ED method, however, one has to take the limit of  $\eta \rightarrow 0^+$  in principle, which leads to  $\delta$ -function peaks in  $\text{Im}\Sigma$  at the zero surfaces of  $G$ . In this limit there is no contribution from the zeros to the Fermi surface region, namely, the closed hole-pocket structure remains robust in the spectral weight and the Fermi arc does not show up, as demonstrated in Fig. 4(a) for a sufficiently small  $\eta$ . In real situations of experiments, however,  $\text{Im}\Sigma$  is broadened through various extrinsic factors, such as temperature, impurity scatterings and phonons [25]. These effects are phenomenologically represented by a broadening to  $\text{Im}\Sigma$  through a nonzero  $\eta$ . In fact, for larger  $\eta$ , the singularities of  $\text{Im}\Sigma$  are smeared out and the spectral weight close to the zeros are suppressed as shown in Fig. 4(b). Thus the Fermi arc is reproduced by introducing a phenomenological broadening factor  $\eta$  in the present result.

To summarize, we have shown that key elements of the Mott physics such as in-gap states, hole pocket, Fermi arc, pseudogap, and Lifshitz transitions result from global reconstructions and interferences of pole and zero surfaces with

doping to the Mott insulator. The reconstructions are caused by a drastic relaxation of the doublon-holon binding at tiny doping. The criticality at  $\delta \rightarrow 0$  and a mechanism of the relaxation, though we have given a qualitative picture, should further be clarified in future studies. It is also desired to confirm our results in calculations for larger clusters.

We thank Y. Z. Zhang for useful comments. SS also thanks S. Watanabe, Y. Yanase, G. Sangiovanni, and D. Tahara for valuable discussions. This work is supported by a Grant-in-Aid for Scientific Research on Priority Areas ‘‘Physics of Superclean Materials’’ from MEXT, Japan.

- 
- [1] M. R. Norman *et al.*, *Nature* **392**, 157 (1998).
  - [2] J. Chang *et al.*, arXiv:0805.0302 (2008).
  - [3] N. Doiron-Leyraud *et al.*, *Nature* **447**, 565 (2007); E. A. Yelland *et al.*, *Phys. Rev. Lett.* **100**, 047003 (2008); A. F. Bangura *et al.*, *ibid.* **100**, 047004 (2008).
  - [4] Y. Yanase *et al.*, *Phys. Rep.* **387**, 1 (2003).
  - [5] R. Preuss, W. Hanke, and W. von der Linden, *Phys. Rev. Lett.* **75**, 1344 (1995); R. Preuss *et al.*, *ibid.* **79**, 1122 (1997).
  - [6] B. Kyung *et al.*, *Phys. Rev. B* **73**, 165114 (2006).
  - [7] E. Dagotto, F. Ortolani, and D. Scalapino, *Phys. Rev. B* **46**, 3183 (1992); P. W. Leung *et al.*, *ibid.* **46**, 11779 (1992); Y. Ohta *et al.*, *ibid.* **46**, 14022 (1992).
  - [8] D. S en echal and A.-M. S. Tremblay, *Phys. Rev. Lett.* **92**, 126401 (2004).
  - [9] A. Macridin *et al.*, *Phys. Rev. Lett.* **97**, 036401 (2006).
  - [10] E. Gull *et al.*, arXiv:0805.3778.
  - [11] M. Civelli *et al.*, *Phys. Rev. Lett.* **95**, 106402 (2005).
  - [12] T. D. Stanescu and G. Kotliar, *Phys. Rev. B* **74**, 125110 (2006); T. D. Stanescu *et al.*, *Ann. Phys. (N. Y.)* **321**, 1682 (2006).
  - [13] K. Haule and G. Kotliar, *Phys. Rev. B* **76**, 104509 (2007).
  - [14] R. M. Konik, T. M. Rice, and A. M. Tsvelik, *Phys. Rev. Lett.* **96**, 086407 (2006); K.-Y. Yang, T. M. Rice, and F.-C. Zhang, *Phys. Rev. B* **73**, 174501 (2006).
  - [15] M. Aichhorn *et al.*, *Phys. Rev. B* **74**, 024508 (2006).
  - [16] I. M. Lifshitz, *Sov. Phys. JETP* **11**, 1130 (1960) [*Zh. Eksp. Teor. Fiz.* **38**, 1569 (1960)]; Y. Yamaji, T. Misawa, and M. Imada, *J. Phys. Soc. Jpn.* **75**, 094719 (2006).
  - [17] T. A. Maier, T. Pruschke, and M. Jarrell, *Phys. Rev. B* **66**, 075102 (2002).
  - [18] Y. Kakehashi and P. Fulde, *Phys. Rev. Lett.* **94**, 156401 (2005).
  - [19] K. Hanasaki and M. Imada, *J. Phys. Soc. Jpn.* **75**, 084702 (2006).
  - [20] I. Dzyaloshinskii, *Phys. Rev. B* **68**, 085113 (2003).
  - [21] E. R. Gagliano and C. A. Balseiro, *Phys. Rev. Lett.* **59**, 2999 (1987).
  - [22] The electronic structure is symmetric around  $\omega = 1.46t$  at  $\delta = 0$  due to the particle-hole symmetry.
  - [23] T. Misawa and M. Imada: *Phys. Rev. B.* **75** 115121 (2007); T. Misawa, Y. Yamaji, and M. Imada, *J. Phys. Soc. Jpn.* **75**, 083705 (2006); M. Imada, *Phys. Rev. B* **72**, 075113 (2005).
  - [24] J. M. Luttinger, *Phys. Rev.* **119**, 1153 (1960).
  - [25] It is also possible that  $\text{Im}\Sigma$  acquires a finite width in the thermodynamic limit while the present calculation, based on finite clusters, cannot reproduce it.